Gold tripyrrindione: Redox chemistry and reactivity with dichloromethane

Clayton J. Curtis^a, Iva Habenšus^a, Jeanet Conradie^{b,c}, Andrey A. Bardin^{d,e},

Brent L. Nannenga^{d,e*}, Abhik Ghosh^{c*}, and Elisa Tomat^{a*}

Abstract

The identification of ligands that stabilize Au(III) centers has led to the isolation of complexes for applications in catalysis, gold-based therapeutics, and functional materials. Herein, we report the coordination of gold by tripyrrin-1,14-dione, a linear tripyrrole with the scaffold of naturally occurring metabolites of porphyrin-based protein cofactors (e.g., heme). Tripyrrindione H₃TD2 binds Au(III) as a trianionic tridentate ligand to form square planar complex [Au(TD2)(H₂O)], which features an adventitious aqua ligand. Two reversible ligand-based oxidations of this complex allow access to the other known redox states of the tripyrrindione framework. Conversely, (spectro)electrochemical measurements and DFT analysis indicate that the reduction of the complex is likely metal-based. The chemical reduction of [Au(TD2)(H₂O)] leads to a reactive species that utilizes dichloromethane in the formation of a cyclometalated organo-Au(III) complex. Both the aqua and the organometallic Au(III) complexes were characterized in the solid state by MicroED methods, which were critical for the analysis of the microcrystalline sample of the organo-gold species. Overall, this study illustrates the synthesis of Au(III) tripyrrindione as well as its redox profile and reactivity leading to gold alkylation chemistry.

^a Department of Chemistry and Biochemistry, The University of Arizona, 1306 E. University Blvd., Tucson, AZ 85721, USA.

^b Department of Chemistry, University of the Free State, Bloemfontein 9300, Republic of South Africa.

^c Department of Chemistry, UiT – The Arctic University of Norway, N-9037 Tromsø, Norway.

^d Center for Applied Structural Discovery, The Biodesign Institute, Arizona State University, Tempe, AZ 85281, USA.

^e Chemical Engineering, School for Engineering of Matter, Transport and Energy, Arizona State University, Tempe, AZ 85287, USA.

Introduction

The coordination chemistry of gold(III) has undergone a remarkable expansion in recent years in the areas of homogeneous catalysis, medicinal chemistry, and materials science. Advances in ligand design have allowed the stabilization of Au(III) complexes in spite of the tendency of Au(III) centers to undergo reduction and form Au(I) species or metallic Au(0).¹ Accordingly, catalytic investigations have benefited from the isolation of important intermediates in catalytic cycles, ²⁻³ including Au(III) hydride and formate complexes.⁴ In drug development, several classes of Au(III) complexes are revealing mechanisms of action that do not rely on the reduction to Au(I) species and well-established reactivity with biological thiolates.⁵⁻⁷ In addition, the luminescence of cyclometalated Au(III) complexes is of significant interest for the development of tunable, robust light-emitting materials.⁸

Tetrapyrrolic macrocycles have been employed for the synthesis of several Au(III) complexes. Porphyrins form stable, cationic Au(III) complexes (e.g., [Au(tpp)]⁺, Chart 1) that have been investigated as anticancer drugs in cultured cells and in animal models. Au(III) corroles (e.g., [Au(TpFPC)], Chart 1) have also been tested as cytotoxic agents and found to serve as triplet photosensitizers in a variety of settings, especially for applications in photovoltaics and photodynamic therapy. Recent findings on gold phlorins further underscore the ability of macrocyclic tetrapyrroles to stabilize Au(III) centers. Here, we sought to investigate the coordination of gold within the tripyrrin-1,14-dione ligand, a linear redox-active tripyrrole that provides a pincer-type tridentate binding unit and leaves an open coordination position in square planar complexes.

Chart 1. Selected tetrapyrrolic Au(III) complexes and tripyrrindione complexes of divalent metals.

The tripyrrin-1,14-dione ligand is a member of the biopyrrin family of linear oligopyrroles, which share the scaffold of naturally occurring pigments deriving from the metabolism of heme and originally isolated from urine.¹³ This ligand promptly undergoes one-electron oxidation upon coordinating divalent transition metals (e.g., Cu(II), Zn(II), Ni(II), Pd(II), Pt(II)) under an aerobic atmosphere.¹⁴⁻¹⁷ The resulting square planar complexes (e.g., [M(TD1*)(H2O)], Chart 1) feature an unpaired spin delocalized on the tripyrrolic ligand and thus far have all demonstrated clear ligand-based redox transformations, undergoing either one-electron oxidation or reduction of the

tripyrrolic π -system. Notably, this redox chemistry is modulated by the monodentate ligand (e.g., aqua, isocyanate, primary amine in [Pt(TD2*)(L)], Chart 1), which also affects the cofacial multicenter interactions between complexes in the solid state and in solution. In this context, we report the synthesis of a Au(III) tripyrrindione complex, along with a detailed (spectro)electrochemical and DFT analysis of its redox chemistry. In particular, this first example of a tripyrrindione complex of a trivalent metal presents a combination of ligand- and metal-based redox processes, with the latter leading to a reactive species capable of engaging dichloromethane as a reaction substrate.

The structural characterization of the complexes in this study was conducted by microcrystal electron diffraction (MicroED). $^{20-21}$ This method was critical for the characterization of one of the gold complexes (*vide infra*), which could only be isolated as extremely thin needles unsuitable for X-ray diffraction analysis. MicroED is a recently developed method that employs a cryogenic transmission electron microscope to collect electron diffraction data. $^{20-21}$ Benefiting from the technology and data processing methods established for electron cryo-microscopy (cryoEM) in structural biology, MicroED allows high-resolution structural analysis of small molecules based on microcrystalline samples that are significantly smaller than those suitable for conventional X-ray diffraction techniques. 22 This study showcases the use of MicroED for the structural analysis of two related Au(III) complexes and particularly of the variation of bond lengths along the delocalized π system of the redox-active tripyrrindione ligand.

Results and discussion

Synthesis and characterization of [Au(TD2)(H₂O)]

The coordination of Au(III) within the tripyrrindione ligand (Scheme 1) was accomplished by heating a DMSO solution of H₃TD2 in the presence of Au(III) acetate and potassium carbonate (3 equiv.) at 60 °C for 45 minutes. The reaction progress was monitored by optical absorption spectroscopy as the mixture turned from orange/red to purple. Once the ligand was fully consumed, aqueous workup and extraction with dichloromethane afforded a crude purple solid, which was purified by column chromatography. The visible absorption spectrum of the isolated complex displays a main absorption maximum at 587 nm (Figure 1). Notably, the near-IR transitions (between 700 and 1000 nm) that characterize complexes of tripyrrindione radicals¹⁴⁻¹⁷ were not observed in this case. Indeed NMR spectroscopic data (Figures S1-S2) indicated that the isolated gold complex is diamagnetic. The ¹H NMR spectrum presented resonances consistent with a symmetric tripyrrindione ligand framework (e.g., one *meso*-type resonance at 6.24 ppm), and a two-hydrogen singlet at 15.45 ppm consistent with the presence of a coordinated aqua ligand as in other complexes of this ligand (Chart 1).

Scheme 1. Synthesis of Au(III) tripyrrin-1,14-dione [Au(TD2)(H₂O)].

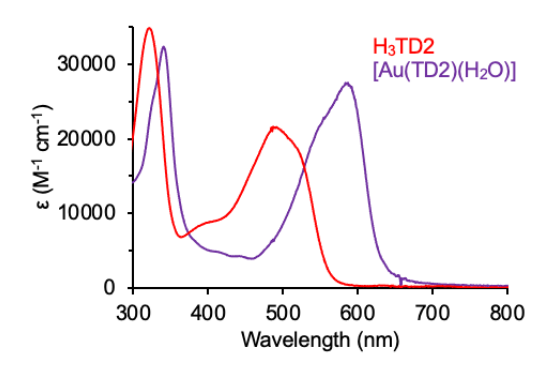


Figure 1. UV-visible absorption spectra of free H₃TD2 and [Au(TD2)(H₂O)] in CH₂Cl₂.

MicroED analysis of a microcrystalline sample of the purple reaction product confirmed the structure of a complex of molecular formula [Au(TD2)(H₂O)], with a square planar geometry around the gold center and a bound agua ligand (Figures 2, S3 and Table S1). The absence of any counter anion, as well as the diamagnetic nature of the complex, indicate that the tripyrrindione ligand is coordinating as a trianionic ligand (TD2³⁻). This finding is in contrast to previous reports on the complexes of hexa-alkyl tripyrrindione bound to divalent metals, which were all isolated as air-stable neutral complexes featuring a dianionic tripyrrindione radical. 14-17 The C-O bond lengths (1.280 and 1.240 Å) of the terminal pyrrolinone rings are consistent with carbon-oxygen double bonds, and comparison of the C-C and C-N bond lengths on the tripyrrindione scaffold to those of neutral [Pd(TD1')(H₂O)] and anionic [Pd(TD1)(H₂O)] complexes¹⁴ (Table S2) further support the trianionic coordination mode assignment for [Au(TD2)(H₂O)]. As in several previously reported tripyrrindione complexes (Chart 1), the aqua ligand is engaged in hydrogen-bonding interactions with the carbonyl oxygen atoms on the tripyrrindione framework (O1–O3, 2.509 Å; O2–O3, 2.376 Å). The Au-aqua bond distance (Au1– O3, 1.993 Å) is within the range of reported Au(III)-OH distances (1.945-2.078 Å) in complexes with pincer ligands²³⁻²⁵ and shorter than the less common Au(III)-OH₂ distances (2.088-2.156) Å). 26-27 The robust hydrogen bonds within the primary coordination sphere of [Au(TD2)(H₂O)] are likely affecting the donating ability and position of the bound agua ligand.

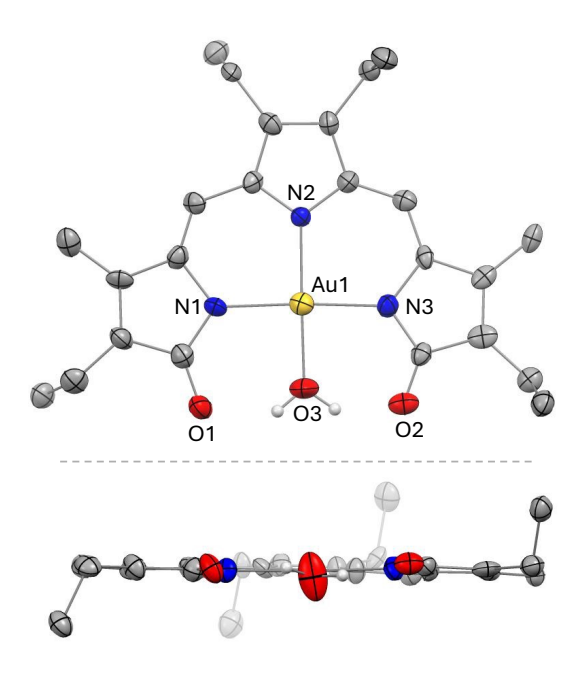


Figure 2. MicroED structure of $[Au(TD2)(H_2O)]$ (top and side views) showing a partial labeling scheme. Carbon-bound hydrogen atoms are omitted for clarity, and non-hydrogen atoms are displayed as thermal displacement ellipsoids set at the 50% probability level. CCDC: 2367152.

Redox properties and DFT analysis of [Au(TD2)(H₂O)]

The cyclic voltammogram of [Au(TD2)(H₂O)] in CH₂Cl₂ presents two reversible oxidations at 0.104 V and 0.660 V along with several irreversible reductive events with a maximum peak current at E_p = -1.010 V, referenced to the ferrocene/ferrocenium (Fc/Fc⁺) couple (Figure 3). Further analysis of the two reversible oxidations by spectroelectrochemical methods allowed their assignment to ligand-based events to generate, respectively, the dianionic radical (i.e., TD2²⁻⁺) and monoanionic (i.e., TD2_{ox}⁻) redox states of the gold-bound tripyrrindione ligand. The formation of the first oxidation product coincided with the growth of three weak near-IR bands between 700-900 nm (Figure S4), which correspond to intraligand π - π charge transfer transitions in complexes of tripyrrindione radicals. The second oxidation then caused a decrease in intensity of these near IR-bands (Figure S4), consistent with the removal of the unpaired spin from the tripyrrindione framework. Overall, these electrochemical data indicate that the trivalent Au(III) center stabilizes the trianionic redox state of the bound tripyrrindione and therefore the ligand-based redox potentials are shifted anodically (by ~700 mV) relative to those of previously reported complexes of divalent metals. ¹⁴⁻¹⁷

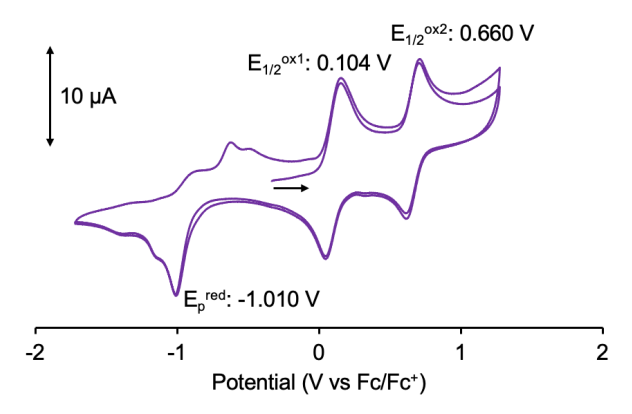


Figure 3. Cyclic voltammogram of [Au(TD2)(H₂O)] at a glassy carbon electrode in CH₂Cl₂ with (NBu₄)(PF₆) as a supporting electrolyte. Data collected at 100 mV s⁻¹ scan rate using a Ag/AgCl pseudoreference electrode and a Pt wire auxiliary electrode.

To further explore its electronic structure, [Au(TD2)(H₂O)] was computationally modeled by scalar-relativistic DFT calculations. Three different functionals were used: OLYP, $^{28-29}$ B3LYP, $^{30-31}$ and B3LYP*, 32 each augmented with Grimme's D3 dispersion corrections, 33 and all with large all-electron Slater-type triple- ζ plus double polarization basis sets. Constraining the symmetry to C_s produced an optimized ground-state geometry with bond lengths in good agreement with the crystallographic data (Figure 4). Table 1 presents calculated adiabatic ionization potentials (IPs), electron affinities (EAs), and singlet-triplet gaps. Additionally, symmetrization to C_s allowed evaluation of the energy of a hypothetical Au(I) excited state, which corresponds to different orbital occupancies across the two irreps of the point group. The quantitative energetics data are generally mutually consistent across the three functionals, with particularly close agreement between B3LYP and B3LYP*. The latter results are thought to be the most accurate based on the excellent track record of DFT calculations in reproducing gas-phase IPs and photoelectron spectra. $^{34-36}$

Given the relatively high EA of the system, it was of interest to determine the energetics of the Au(I) valence tautomer of [Au(TD2)(H₂O)] with the tripyrrindione ligand in a monoanionic state. These relative energy values turned out to be on the order of 1 eV (Table 1), with the coordinated water molecule detaching from the metal center in these states. The Au(III) ground state is clearly preferred, matching our assignment based on experimental data. These calculations underscored the critical importance of relativistic effects, which significantly elevate 5d orbital energies relative to 4d orbital energies for isoelectronic 4d transition metal complexes.³⁷⁻³⁸ Indeed, nonrelativistic calculations on these systems incorrectly predict nearly equienergetic Au(I) and Au(III) states, a key consideration for anyone attempting to model the redox chemistry of gold complexes.

Table 1. DFT adiabatic energetics (eV) of $[Au(TD2)(H_2O)]$ (C_s) for different exchange-correlation functionals: ionization potential (IP), electron affinity (EA), singlet-triplet gap (E_{S-T}), and relative energy of the Au(I) valence tautomer ($E_{Au(I)}$).

| Functional | IP | EA | E s-T | E _{Au(I)} |
|------------|------|------|--------------|--------------------|
| OLYP | 5.84 | 1.97 | 0.42 | 0.70 ^a |
| B3LYP | 5.99 | 2.19 | 0.30 | 0.64ª |
| B3LYP* | 5.97 | 2.11 | 0.39 | 0.75 ^a |

^a The agua ligand has detached in the modeled Au(I) valence tautomer.

The calculations reveal relatively unremarkable IPs (Table 1), about 0.5 eV lower than those for the free-base tetraphenylporphyrin, 34-35 reflecting the relative ease of ionization from the tripyrrindione π-system. Visualization of the HOMO of the neutral complex [Au(TD2)(H₂O)] as well as the spin density of the cationic complex [Au(TD2)(H₂O)]⁺ (Figure 4) indeed displays spin localization on the tripyrrolic ligand, consistent with our spectroelectrochemical data. In contrast, the EAs of [Au(TD2)(H₂O)] are rather high, a few to several hundreds of meV higher than that of a typical electronically innocent metalloporphyrin, ³⁹ possibly reflecting a metal-centered reduction. The spin density profile of the anionic state [Au(TD2)(H₂O)]⁻ depicts localization of the unpaired spin on the metal and within the primary coordination sphere and is mirrored by the LUMO of the parent complex, which shows a similar distribution (Figure 4). In this respect, [Au(TD2)(H₂O)] appears analogous to cationic Au(III) porphyrins, which are also known to undergo Au-centered reduction. 40-44 Notably, in the case of Au(III) phlorin, both the LUMO and the first reduction event are partially gold-centered as a result of metal-ligand orbital mixing due to inherent ruffling of the phlorin macrocycle. 12 The reduction of Au(III) corroles is instead ligand-centered. 11, 45 further showcasing the ability of oligopyrrolic ligands to modulate the electronic structure of Au(III) complexes.

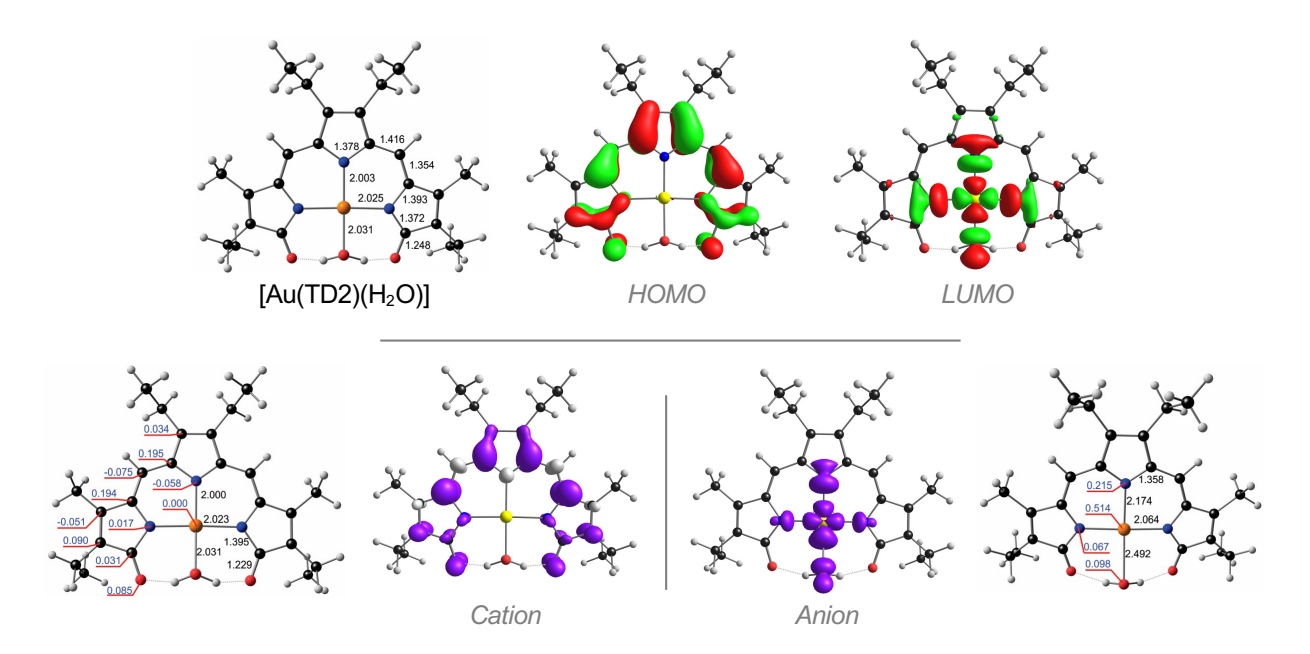


Figure 4. Selected B3LYP-D3/ZORA-STO-TZ2P results for [Au^{III}(TD2)(H₂O)] optimized within the C_s point group. Bond distances (Å) are indicated in black. Mulliken spin populations are indicated in blue and with red underlining. Bottom row: spin density plots of the ionized states.

Chemical reduction of [Au(TD2)(H₂O)] and reactivity with CH₂Cl₂

The metal character of the calculated LUMO and spin density of anionic $[Au(TD2)(H_2O)]^-$ (Figure 4) prompted us to examine the reduction of $[Au(TD2)(H_2O)]$. By spectroelectrochemical methods, a blue shift in the λ_{max} to 578 nm was observed upon controlled potential electrolysis in CH_2CI_2 at -1.2 V (Figure 5a). The electrochemical data are very similar when collected in THF (Figure S5); however, a small shoulder around 630 nm only appeared in CH_2CI_2 and this observation was further investigated upon chemical reduction (*vide infra*). Overall, the limited spectral changes upon electrochemical one-electron reduction, and especially the absence of any new near-IR transitions, suggested a metal-based redox process.

The chemical reduction of [Au(TD2)(H₂O)] with CoCp₂ (1.0 equiv or sub-stoichiometric amounts) to isolate the burgundy red product observed via spectroelectrochemistry was conducted in a variety of experimental conditions. In chloroform, acetonitrile, toluene, and THF under an inert atmosphere, the formation of a red product was observed, but this species presented limited stability and could not be reproducibly characterized by spectroscopic and crystallographic methods. The formation of an intractable precipitate degradation/demetalation in several cases. Continuous-wave EPR experiments were attempted both at room temperature and after flash-freezing at 77 K or 10 K: a weak axial signal was observed but did not clearly indicate the presence of a Au(II) species. For instance, the EPR spectrum of Au(II) tetraphenylporphyrin presents hyperfine couplings to 197 Au (I = 3/2) and to the ¹⁴N donors. ^{40, 42}

When the chemical reduction of [Au(TD2)(H₂O)] was conducted in dichloromethane, the reaction mixture underwent a color change from purple to burgundy red and then, within a few

minutes, to blue. The reaction product was purified by crystallization and isolated in good yield (71%) from a solution of dichloromethane and pentane. The isolated blue solid was found to be air-stable and diamagnetic. No other product was observed when extending the reaction time. The optical absorption spectrum of the isolated complex is characterized by a sharp band at 635 nm (Figure S6). Its ¹H NMR spectrum (Figure S7) is indicative of an asymmetric tripyrrindione ligand scaffold, with two *meso*-type 1H singlets at 6.17 and 7.02 ppm, along with four ethyl 2H quartets between 2.40 and 2.75 ppm. Additionally, the resonance corresponding to the bound aqua ligand in the parent complex at 15.45 ppm was absent and replaced by a new sharp 2H singlet at 6.79 ppm. A ¹³C NMR signal correlating to this resonance was observed at 82.3 ppm (assigned by HSQC NMR, Figures S8-S9) and suggested the presence of a methylene moiety. Similar NMR resonances were observed for a cyclometalated complex isolated upon Pd(II) coordination with a 1,14-dimethoxytripyrrin ligand. ⁴⁶ High-resolution mass spectrometry analysis also supported the formation of a cyclometalated species in which a methylene bridge is covalently linked to one terminal oxygen atom of the tripyrrindione ligand and occupies the fourth site within the primary coordination sphere (Scheme 2).

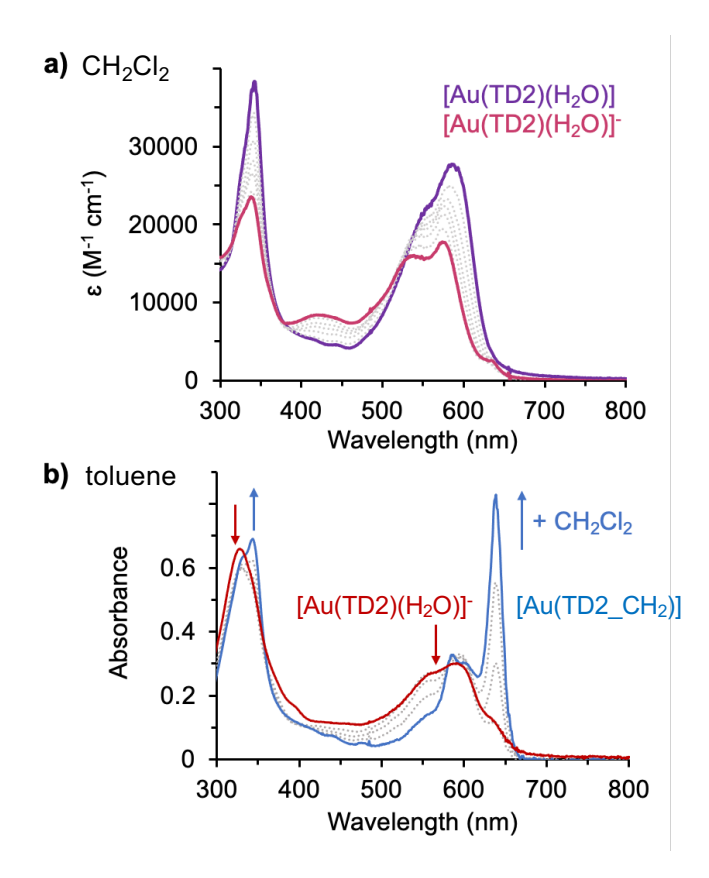


Figure 5. Reduction and reactivity of [Au(TD2)(H₂O)]. a) Spectral changes observed upon reduction of [Au(TD2)(H₂O)] (purple trace) by controlled potential electrolysis at -1.2 V in CH₂Cl₂ (with 0.1 M (NBu₄)(PF₆) as supporting electrolyte) to produce the one-electron reduction product (red trace). b) Spectral changes recorded for a solution of [Au(TD2)(H₂O)]⁻ (200 μM, generated *in situ*) in toluene (red trace) upon addition of CH₂Cl₂ (100 μL) to form [Au(TD2_CH₂)] over 20 min.

Scheme 2. Chemical reduction and reactivity of [Au(TD2)(H₂O)] in dichloromethane.

To further confirm the reactivity with CH_2CI_2 proposed in Scheme 2, we generated the reduction product $[Au(TD2)(H_2O)]^-$ in toluene under an inert atmosphere and then added excess CH_2CI_2 as a reagent. In these conditions at room temperature, we observed the gradual formation of the same blue product $[Au(TD2_CH_2)]$ over the course of 20 min (Figure 5b). When performed in deuterated dichloromethane under identical conditions, this reaction again afforded a blue complex with the same UV-vis absorption profile, and the formation of the deuterated $[Au(TD2_CD_2)]$ product was confirmed by 1H NMR and HRMS analysis. The 1H NMR spectrum displayed essentially identical resonances for the asymmetric tripyrrindione ligand as observed for $[Au(TD2_CH_2)]$; however, the 2H singlet at 6.79 ppm attributed to the Au-bound methylene unit was absent (Figure S10).

Because our crystals of [Au(TD2_CH₂)] were too small for single-crystal X-ray diffractometry, we sought to elucidate the structure by MicroED. Crystals grew as thin needles (i.e., $5 \times 0.3 \times -0.05 \,\mu$ m) from slow diffusion of hexane into a solution of [Au(TD2_CH₂)] in CH₂Cl₂. The structure, which is obtained by merging multiple sets of electron diffraction data from different crystals, ²⁰⁻²¹ confirms the insertion of a methylene group forming a cyclometalated complex (Figure 6). The ligand coordinates in trianionic, tetradentate fashion with one terminal pyrrolic nitrogen binding as a neutral iminic donor. This change along the tripyrrindione π system is evident when comparing bond metrics. The C1–O1 bond involved in the cyclometalated ring (1.321 Å) is significantly longer than the C14–O2 double bond (1.245 Å) typical of carbonyl termini in tripyrrindiones. The iminic N1–C1 bond (1.361 Å) is shorter than the N2-C14 single bond (1.407 Å), indicating a significant change in the conjugation of the ligand π system.

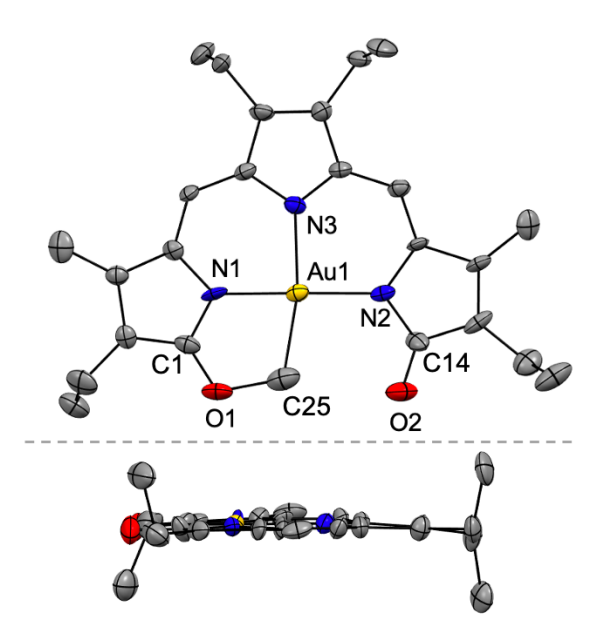


Figure 6. MicroED structure of [Au(TD2_CH₂)] (top and side views) showing a partial labeling scheme. Carbon-bound hydrogen atoms are omitted for clarity, and non-hydrogen atoms are displayed as thermal displacement ellipsoids at the 50 % probability level. CCDC: 2367161.

Based on our electrochemical and computational analyses, the reduction of the parent complex [Au(TD2)(H₂O)] was tentatively assigned as metal-centered. Indeed Au(II) intermediates and subsequent formation of organo-Au(III) species have been proposed in the rapidly expanding field of gold-based redox (photo)catalysis. Alternatively, the redox-noninnocence of the ligand could allow stabilization of a Au(I) valence tautomer, in which the tripyrrindione hosts an unpaired spin and the aqua ligand would likely detach as indicated by our DFT calculations for the parent compound (Table 1). The reactivity of putative complex [Au^I(TD2*)]⁻ would then be analogous to that of unusually nucleophilic Au(I) centers. Ale-50 In fact the alkylation of Au(I) with dichloromethane and formation of Au(III) species was also observed in complexes of pincer ligands with mesoionic carbene donors. Overall, our observations on the reactivity of the parent gold tripyrrindione [Au(TD2)(H₂O)] with dichloromethane upon reduction are consistent with the formation of a gold species in a lower oxidation state and therefore with a metal-based reduction.

Redox properties and DFT analysis of [Au(TD2_CH₂)]

The cyclic voltammogram of [Au(TD2_CH₂)] (Figure 7) displays two reversible oxidations at potentials similar to those of the aqua-bound precursor. When analyzed by spectroelectrochemical methods (Figure S11), the two oxidations were found to be analogous to those of the aqua-bound parent complex (Figure S4), corresponding to two successive one-electron oxidation events primarily localized on the tripyrrolic ligand π -system. In addition, a new reversible reduction was observed at a highly shifted potential (-1.812 V vs Fc/Fc⁺, Figure 7) that could not be maintained to attain complete conversion with our spectroelectrochemical setup.

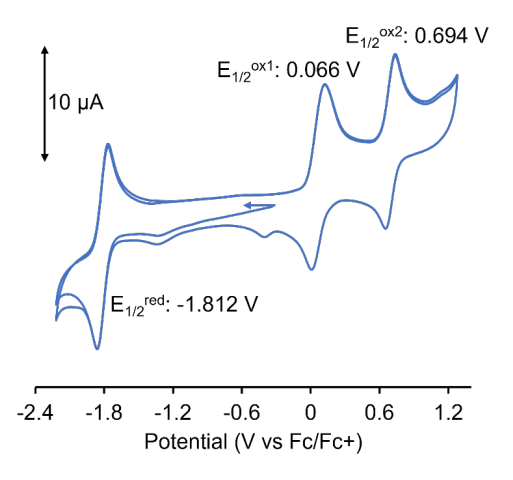


Figure 7. Cyclic voltammogram of [Au(TD2_CH₂)] at a glassy carbon electrode in CH₂Cl₂ with (NBu₄)(PF₆) as a supporting electrolyte. Data collected at 100 mV s⁻¹ scan rate using a Ag/AgCl pseudoreference electrode and a Pt wire auxiliary electrode.

To gain further insight into its electronic structure, the asymmetric [Au(TD2_CH2)] complex was computationally modeled in a similar manner to [Au(TD2)(H2O)] using the OLYP, B3LYP, and B3LYP* functionals. The optimized geometry (Figure 8) for the full structure [Au(TD2_CH2)] was determined with B3LYP, and the IPs were mostly consistent among the three functionals (Table 2). The IPs of [Au(TD2_CH2)] were very similar to those determined for [Au(TD2)(H2O)], reflecting the consistency of their electrochemical profiles upon oxidation of the tripyrrolic ligand. Indeed the HOMO of [Au(TD2_CH2)] and the spin density profile of the cationic state similarly display localization on the tripyrrin π -system (Figure 8). Simplification of the asymmetric [Au(TD2_CH2)] complex to [Au(TD2s_CH2)], where the ethyl groups have been replaced by methyl groups, and symmetrization to C_s allowed us to evaluate the comparative energetics of metal- versus ligand-centered reduction (as these correspond to electron addition to MOs with different irreps). In contrast to [Au(TD2)(H2O)], the calculations revealed relatively low EAs of approximately 1.4 eV for [Au(TD2_CH2)] and [Au(TD2s_CH2)], about the same as that observed for electronically innocent metalloporphyrins, 39 reflecting a ligand-centered reduction.

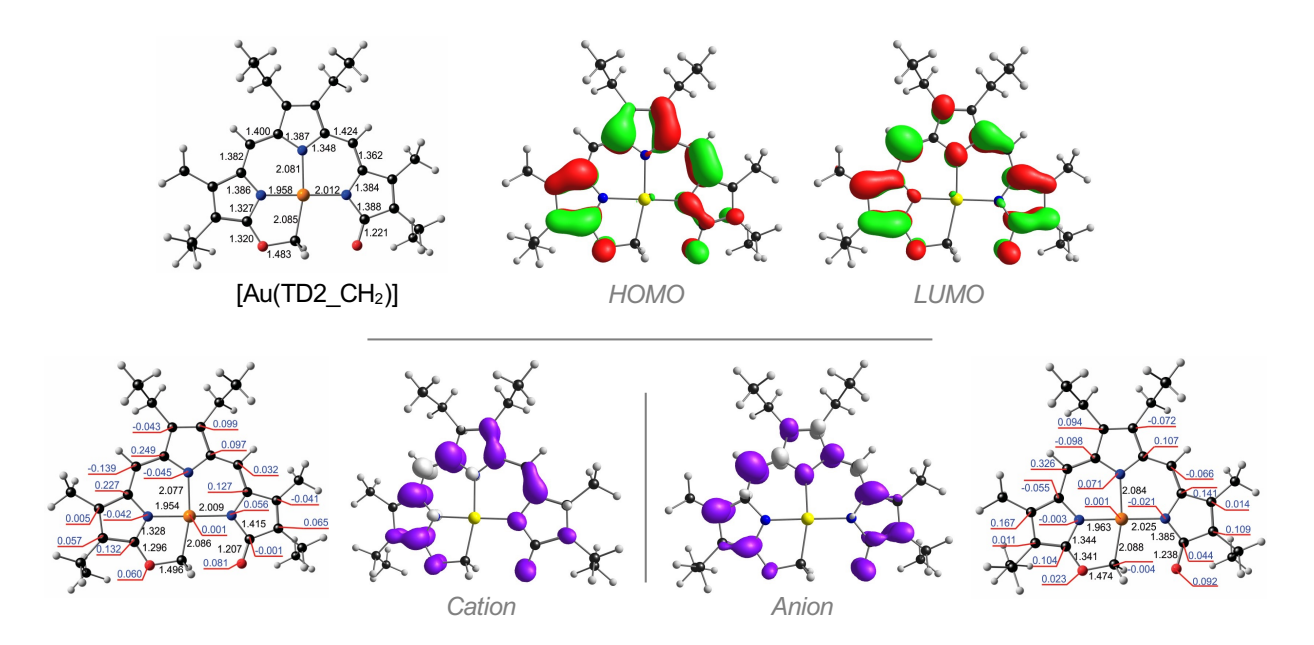


Figure 8. Selected B3LYP-D3/ZORA-STO-TZ2P results for [Au^{III}(TD2_CH₂)] optimized with no symmetry constraints. Bond distances (Å) are indicated in black. Mulliken spin populations are indicated in blue and with red underlining. Bottom row: spin density plots for ionized states.

Table 2. DFT adiabatic energetics (eV) of model complexes of $[Au(TD2-CH_2)]$ for different exchange-correlation functionals: ionization potential (IP), electron affinity (EA), singlet-triplet gap (E_{S-T}).

| Complex | Functional | IP | EA | E s₋⊤ |
|--|------------|------|------------------------|--------------|
| Au[TD2_CH ₂] (C ₁) | OLYP | 5.85 | 1.27 | 1.13 |
| | B3LYP | 6.02 | 1.39 | 1.18 |
| | B3LYP* | 5.97 | 1.40 | 1.12 |
| $Au[TD2s_CH_2]^a (C_s)$ | OLYP | 5.90 | 1.24/-b | 1.12 |
| | B3LYP | 6.06 | 1.37/0.70 ^b | 1.18 |
| | B3LYP* | 6.02 | 1.36/0.68 ^b | 1.12 |

^a The peripheral ethyl groups in the experimentally studied complex have been simplified to methyls in this complex.

For the symmetrized complex, an adiabatic EA for Au-centered electron addition was also calculated: the resulting value, about 0.7 eV, shows that Au-centered reduction is unfavorable for [Au(TD2_CH₂)], possibly reflecting its much stronger ligand field in comparison to the aqua-bound complex. High singlet-triplet gaps of over 1 eV also lead to the same conclusion. In these respects, the electronic characteristics of [Au(TD2_CH₂)] and [Au(TD2s_CH₂)] mirror those of Au(III) corroles, which also undergo corrole-centered reduction.⁵¹⁻⁵²

^b The second, adiabatic EAs refer to Au-centered electron addition.

Conclusions

We synthesized a Au(III) tripyrrin-1,14-dione complex as the first example of this ligand bound to a trivalent metal. In contrast to prior studies featuring divalent metals, wherein the tripyrrolic ligand coordinates as a dianionic radical, we have shown through a combination of spectroscopic, crystallographic, and computational techniques that tripyrrindione coordinates trivalent gold as a trianionic ligand in [Au(TD2)(H₂O)]. Electrochemical analysis by cyclic voltammetry and spectroelectrochemical methods revealed that the coordinated tripyrrindione ligand undergoes two quasi-reversible one-electron oxidation events that are characteristic of previously studied complexes. Furthermore, an irreversible reduction was observed at -1.01 V (vs Fc/Fc⁺) and attributed to a metal-based event based on spectroelectrochemical and computational analyses. The reduced complex was found to react with dichloromethane and form a cyclometalated organo-gold(III) complex, which was characterized in solution by NMR spectroscopy and in the solid state by MicroED. This asymmetric tripyrrin complex features a methylene moiety bound to the Au(III) center and to a terminal oxygen of the tripyrrindione framework. The air-stable, diamagnetic [Au(TD2 CH₂)] complex undergoes successive ligand-based one-electron oxidations at potentials similar to its aqua precursor. Additionally, voltammetry and DFT calculations revealed the presence of a quasi-reversible reduction at a much more anodic potential (-1.812 V). In contrast to the reduction of its agua precursor, comparison of the calculated EAs for this complex indicated that this event is also ligand-based, likely on account of the stronger ligand field of the alkyl donor. This work overall reports two complexes featuring tripyrrolic ligands bound to trivalent gold centers that undergo a combination of ligand- or metalcentered redox transformations dictated by the identity of the moiety occupying the fourth coordination site. Although further exploration of their reactivity is warranted, this study indicated that the one-electron reduction of [Au(TD2)(H₂O)] leads to a highly reactive species that engages dichloromethane as a reagent for the formation of an alkylated Au(III) complex.

EXPERIMENTAL

Materials and Methods. The H₃TD2 ligand was synthesized following a previously published procedure. ¹⁹ Dichloromethane (CH₂Cl₂) and pentane were dried by passage through a solvent purifier. Dry solvents were confirmed to contain <0.1 ppm H₂O using a Mettler Toledo C10S Coulometric Karl Fisher Titrator. All other solvents and commercial reagents were used without further purification. Aluminum-backed silica gel plates (thickness: 200 μm) were used to monitor reactions by thin layer chromatography (TLC). Chromatographic purifications on silica gel were conducted on a Biotage Isolera One Flash instrument. NMR spectra were recorded on a Bruker Advance-III 400 MHz and a Bruker NEO-500 MHz NMR spectrometer at the University of Arizona Department of Chemistry and Biochemistry NMR Facility (RRID: SCR_012716). UV-visible absorption spectra were obtained at ambient temperature using an Agilent Cary 60 spectrophotometer. High-resolution mass spectra (HRMS) *via* electrospray ionization (ESI) methods were obtained at University of Arizona Analytical & Biological Mass Spectrometry Facility (RRID: SCR_023370). Elemental analyses were performed by NuMega Resonance Laboratories in San Diego, CA.

Synthetic Procedures

[Au(TD2)(H₂O)]. H₃TD2 (11.0 mg, 0.028 mmol), Au(OAc)₃ (18.6 mg, 0.050 mmol), and K₂CO₃ (11.3 mg, 0.082 mmol) were dissolved in DMSO (0.8 mL) and heated at 60 °C for 45 minutes. Upon consumption of H₃TD2 (as determined by UV-visible absorption spectroscopy), the reaction mixture was cooled to room temperature and diluted with CH₂Cl₂ (20 mL). The mixture was then transferred to a separatory funnel and washed with brine (3 x 20 mL). The organic phase was dried over Na₂SO₄, and the solvent was removed under reduced pressure. The crude solid was purified *via* flash chromatography (0/100 to 30/70, v/v, ethyl acetate/hexanes) to afford [Au(TD2)(H₂O)] as a purple solid (5.4 mg, 32%). UV-vis (CH₂Cl₂) λ_{max} (ε): 341 (31,200), 587 (27,300 M⁻¹ cm⁻¹). ¹H NMR (500 MHz, CDCl₃): δ 15.51 (s, 2H), 6.28 (s, 2H), 2.53 (q, J = 7.5 Hz, 4H), 2.36 (q, J = 7.6 Hz, 4H), 2.14 (s, 6H), 1.13 (m, 12H); ¹³C NMR (125 MHz, CDCl₃): 178.6, 137.9, 133.7, 132.1, 131.8, 128.6, 104.0, 17.9, 17.3, 17.0, 13.7, 9.5. HRMS-ESI⁺ (m/z): [M]⁺ calcd. for [C₂₄H₃₀AuN₃O₂], 605.19527; found, 605.19503. Anal. calcd. for [C₂₄H₃₀AuN₃O₃]: C, 47.6; H, 5.0; N, 6.9 %; found: C, 47.3; H, 4.6; N, 7.0 %.

[Au(TD2_CH₂)]. Complex [Au(TD2)(H₂O)] (4.1 mg, 0.0068 mmol) was dissolved in CH₂Cl₂ (1.5 mL) in a nitrogen-filled glovebox. After addition of 1.0 equiv. of CoCp₂ (1.3 mg, 0.0068 mmol), the reaction mixture was allowed to stir at room temperature for 10 minutes. Within this time, the color of the mixture changed from purple to teal blue. The solvent was then removed under reduced pressure and the crude blue solid was redissolved in CH₂Cl₂, filtered through glass wool, and layered with pentane to afford thin blue needles of [Au(TD2_CH₂)] (2.9 mg, 71%). UV-vis (CH₂Cl₂) λ_{max} (ε): 345 (23,300), 585 (14,100), 636 (39,600 M⁻¹ cm⁻¹). ¹H NMR (500 MHz, CDCl₃): δ 7.02 (s, 1H), 6.79 (s, 2H), 6.17 (s, 1H), 2.71 (q, J = 7.6 Hz, 2H), 2.65 (q, J = 7.6 Hz, 2H), 2.53 (q, J = 7.6 Hz, 2H), 2.44 (q, J = 7.3 Hz, 2H), 1.19 (m, 12H). ¹³C NMR (125 MHz, CDCl₃): 179.4, 140.3, 139.7, 139.3, 139.1, 138.6, 137.6, 134.0, 130.6, 130.3, 122.6, 117.4, 115.1, 97.4, 82.3, 18.1, 17.8, 17.7, 17.6, 17.3, 16.5, 14.0, 13.6, 10.3, 10.0. HRMS-ESI⁺ (m/z): [M+H]⁺ calcd. for [C₂₅H₃₁AuN₃O₂], 602.2076; found, 602.2062; and calcd. for [C₂₅H₂₉D₂AuN₃O₂], 604.2202; found, 604.2200. Anal. calcd. for [C₂₅H₃₀AuN₃O₃•C₅H₁₂]: C, 53.5; H, 6.3; N, 6.2 %; found: C, 53.0; H, 5.9; N, 6.1 %.

MicroED Analysis. Samples were prepared for MicroED analysis by pipetting 2 μL of microcrystalline suspension onto the surface of a lacey carbon coated EM grid. The solvent was allowed to evaporate from the surface of the grids prior to loading into a Titan Krios cryo-TEM, which was cooled to liquid-nitrogen temperature and operated at 300 kV. MicroED data were collected on a Ceta-D camera with a stage rotation rate of 0.5° per second and a camera integration time of 2 seconds, leading to diffraction images corresponding to 1° per frame. For each sample, multiple crystals were merged together to improve data completeness. MicroED data were processed using XDS,⁵³ and the structure solution was determined using SHELXT (v. 2018/2).⁵⁴ The structures of complexes [Au(TD2)H₂O] and [Au(TD2_CH₂)] were refined using Olex2 (v1.5).⁵⁵⁻⁵⁶

Electrochemical Analysis. Cyclic voltammograms were performed on a Gamry Reference 600 potentiostat utilizing a single-compartment cell with three electrodes: a glassy carbon working electrode, a platinum wire auxiliary electrode, and a Ag/AgNO₃ quasi-reference electrode. Measurements were performed at ambient temperature under an inert argon atmosphere in CH₂Cl₂ containing 0.1 M (NBu₄)(PF₆) (triply recrystallized) as a supporting electrolyte. Sample concentrations were 1–2 mM, and all electrochemical data were internally referenced to the ferrocene/ferrocenium couple (set at 0.00 V).

Computational Methods. Scalar-relativistic DFT calculations with the ZORA Hamiltonian⁵⁷⁻⁵⁸ and all-electron STO-TZ2P ZORA basis sets were carried out with the OLYP²⁸⁻²⁹ and B3LYP⁵⁹ (20% exchange), each augmented with D3 dispersion corrections,³³ all as implemented ADF program system.⁶⁰ Carefully tested, fine integration grids and tight SCF and geometry optimization criteria were used throughout.

ASSOCIATED CONTENT

Supporting Information

The Supporting Information is available free of charge on the ACS Publications website.

Supplementary NMR and (spectro)electrochemical data, details of structural and computational analyses (PDF)

AUTHOR INFORMATION

Corresponding Authors

* Elisa Tomat (tomat@arizona.edu), Abhik Ghosh (abhik.ghosh@uit.no), Brent Nannenga (Brent.Nannenga@asu.edu)

Author Contributions

The manuscript was written through contributions of all authors. All authors have given approval to the final version of the manuscript.

Funding Sources

This work was supported by the National Science Foundation (awards CHE-2203361 to E.T. and DMR-1942084 to D.L.N). We also acknowledge additional support from the National Institutes of Health (award P41 GM136508 to B.N.L.), the Research Council of Norway (grant 262229 to A.G.), and the South African National Research Foundation (grants 129270 and 132504 to J.C.)

ACKNOWLEDGMENT

We acknowledge the use of the Titan Krios at the Eyring Materials Center at Arizona State University and the funding of this instrument by NSF MRI 1531991. We thank Dr. Andrei Astashkin at the University of Arizona Electron Paramagnetic Resonance Facility for assistance during multiple attempts to characterize a paramagnetic reduction product.

REFERENCES

Preprints: Curtis, C. J.; Habenšus, I.; Conradie, J.; Bardin, A. A..; Nannenga, B. L.; Ghosh, A.; Tomat, E. Gold tripyrrindione: Redox chemistry and reactivity with dichloromethane, ChemRxiv (Inorganic Chemistry), 2024-07-12, DOI: 10.26434/chemrxiv-2024-wx1m3.

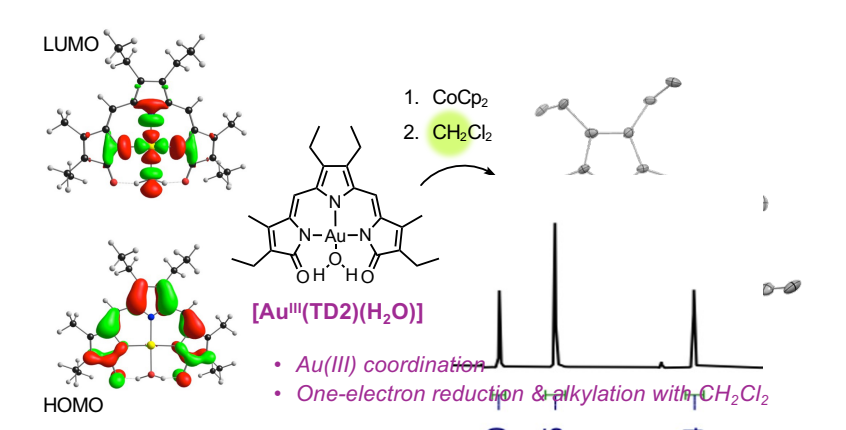
- 1. Kumar, R.; Nevado, C., Cyclometalated Gold(III) Complexes: Synthesis, Reactivity, and Physicochemical Properties. *Angew. Chem. Int. Ed.* **2017**, *56*, 1994-2015.
- 2. Rocchigiani, L.; Bochmann, M., Recent Advances in Gold(III) Chemistry: Structure, Bonding, Reactivity, and Role in Homogeneous Catalysis. *Chem. Rev.* **2021,** *121,* 8364-8451.
- 3. Huang, B.; Hu, M.; Toste, F. D., Homogeneous Gold Redox Chemistry: Organometallics, Catalysis, and Beyond. *Trends Chem.* **2020**, *2*, 707-720.
- 4. Martín, J.; Schörgenhumer, J.; Biedrzycki, M.; Nevado, C., (P^N^C) Ligands to Stabilize Gold(III): A Straightforward Access to Hydroxo, Formate, and Hydride Complexes. *Inorg. Chem.* **2024**, 63, 8390-8396.
- 5. Moreno-Alcántar, G.; Picchetti, P.; Casini, A., Gold Complexes in Anticancer Therapy: From New Design Principles to Particle-Based Delivery Systems. *Angew. Chem. Int. Ed.* **2023**, *62*, e202218000.
- 6. Mertens, R. T.; Gukathasan, S.; Arojojoye, A. S.; Olelewe, C.; Awuah, S. G., Next Generation Gold Drugs and Probes: Chemistry and Biomedical Applications. *Chem. Rev.* **2023**, *123*, 6612-6667.
- 7. Salmain, M.; Bertrand, B., Emerging Anticancer Therapeutic Modalities Brought by Gold Complexes: Overview and Perspectives. *Eur. J. Inorg. Chem.* **2023**, *26*, e202300340.
- 8. Tang, M.-C.; Chan, M.-Y.; Yam, V. W.-W., Molecular Design of Luminescent Gold(III) Emitters as Thermally Evaporable and Solution-Processable Organic Light-Emitting Device (OLED) Materials. *Chem. Rev.* **2021**, *121*, 7249-7279.
- 9. Sun, R. W.-Y.; Che, C.-M., The anti-cancer properties of gold(III) compounds with dianionic porphyrin and tetradentate ligands. *Coord. Chem. Rev.* **2009**, *253*, 1682-1691.
- 10. Teo, R. D.; Hwang, J. Y.; Termini, J.; Gross, Z.; Gray, H. B., Fighting Cancer with Corroles. *Chem. Rev.* **2017**, *117*, 2711-2729.
- 11. Alemayehu, A. B.; Thomas, K. E.; Einrem, R. F.; Ghosh, A., The Story of 5d Metallocorroles: From Metal–Ligand Misfits to New Building Blocks for Cancer Phototherapeutics. *Acc. Chem. Res.* **2021**, *54*, 3095-3107.
- 12. Larsen, S.; Adewuyi, J. A.; Thomas, K. E.; Conradie, J.; Rousselin, Y.; Ung, G.; Ghosh, A., Electronic Structure of Metallophlorins: Lessons from Iridium and Gold Phlorin Derivatives. *Inorg. Chem.* **2024**, *63*, 9842-9853.
- 13. Tomat, E.; Curtis, C. J., Biopyrrin Pigments: From Heme Metabolites to Redox-Active Ligands and Luminescent Radicals. *Acc. Chem. Res.* **2021**, *54*, 4584-4594.
- 14. Gautam, R.; Loughrey, J. J.; Astashkin, A. V.; Shearer, J.; Tomat, E., Tripyrrindione as a Redox-Active Ligand: Palladium(II) Coordination in Three Redox States. *Angew. Chem. Int. Ed.* **2015**, *54*, 14894-14897.
- 15. Bahnmüller, S.; Plotzitzka, J.; Baabe, D.; Cordes, B.; Menzel, D.; Schartz, K.; Schweyen, P.; Wicht, R.; Bröring, M., Hexaethyltripyrrindione (H3Et6tpd): A Non-Innocent Ligand Forming Stable Radical Complexes with Divalent Transition-Metal Ions. *Eur. J. Inorg. Chem.* **2016**, 4761–4768.
- Gautam, R.; Petritis, S. J.; Astashkin, A. V.; Tomat, E., Paramagnetism and Fluorescence of Zinc(II) Tripyrrindione: A Luminescent Radical Based on a Redox-Active Biopyrrin. *Inorg. Chem.* 2018, 57, 15240-15246.

- 17. Gautam, R.; Astashkin, A. V.; Chang, T. M.; Shearer, J.; Tomat, E., Interactions of Metal-Based and Ligand-Based Electronic Spins in Neutral Tripyrrindione π Dimers. *Inorg. Chem.* **2017,** *56*, 6755-6762.
- 18. Habenšus, I.; Ghavam, A.; Curtis, C. J.; Astashkin, A. V.; Tomat, E., Primary amines as ligands and linkers in complexes of tripyrrindione radicals. *J. Porphyrins Phthalocyanines* **2023**, *27*, 1448-1456.
- 19. Tomat, E.; Curtis, C. J.; Astashkin, A. V.; Conradie, J.; Ghosh, A., Multicenter interactions and ligand field effects in platinum(II) tripyrrindione radicals. *Dalton Trans.* **2023**, *52*, 6559-6568.
- 20. Nannenga, B. L.; Gonen, T., The cryo-EM method microcrystal electron diffraction (MicroED). *Nat. Methods* **2019**, *16*, 369-379.
- 21. Haymaker, A.; Nannenga, B. L., Advances and applications of microcrystal electron diffraction (MicroED). *Curr. Opin. Struct. Biol.* **2024**, *84*, 102741.
- 22. Jones, C. G.; Martynowycz, M. W.; Hattne, J.; Fulton, T. J.; Stoltz, B. M.; Rodriguez, J. A.; Nelson, H. M.; Gonen, T., The CryoEM Method MicroED as a Powerful Tool for Small Molecule Structure Determination. *ACS Centr. Sci.* **2018**, *4*, 1587-1592.
- 23. Pitteri, B.; Marangoni, G.; Visentin, F.; Bobbo, T.; Bertolasi, V.; Gilli, P., Equilibrium and kinetic studies of (2,2':6',2"-terpyridine)gold(III) complexes. Preparation and crystal structure of [Au(terpy)(OH)][CIO4]2. *J. Chem. Soc., Dalton Trans.* **1999**, 677-682.
- 24. Roşca, D.-A.; Smith, D. A.; Bochmann, M., Cyclometallated gold(III) hydroxides as versatile synthons for Au–N, Au–C complexes and luminescent compounds. *Chem. Commun.* **2012**, 48, 7247-7249.
- Engbers, S.; Trifonova, E. A.; Hess, K. M.; de Vries, F.; Klein, J. E. M. N., Synthesis of a Sterically Encumbered Pincer Au(III)-OH Complex. Eur. J. Inorg. Chem. 2021, 2021, 3561-3564.
- 26. Zhukhovitskiy, A. V.; Kobylianskii, I. J.; Wu, C.-Y.; Toste, F. D., Migratory Insertion of Carbenes into Au(III)–C Bonds. *J. Am. Chem. Soc.* **2018**, *140*, 466-474.
- Kim, S.; Toste, F. D., Mechanism of Photoredox-Initiated C–C and C–N Bond Formation by Arylation of IPrAu(I)–CF3 and IPrAu(I)–Succinimide. *J. Am. Chem. Soc.* 2019, 141, 4308-4315.
- 28. Handy, N. C.; Cohen, A. J., Left-right correlation energy. *Mol. Phys.* **2001**, 99, 403-412.
- 29. Lee, C.; Yang, W.; Parr, R. G., Development of the Colle-Salvetti correlation-energy formula into a functional of the electron density. *Phys. Rev. B* **1988**, *37*, 785-789.
- 30. Becke, A. D., Density-functional exchange-energy approximation with correct asymptotic behavior. *Phys. Rev. A* **1988**, *38*, 3098-3100.
- 31. Miehlich, B.; Savin, A.; Stoll, H.; Preuss, H., Results obtained with the correlation energy density functionals of becke and Lee, Yang and Parr. *Chem. Phys. Lett.* **1989**, *157*, 200-206
- 32. Reiher, M.; Salomon, O.; Artur Hess, B., Reparameterization of hybrid functionals based on energy differences of states of different multiplicity. *Theor. Chem. Acc.* **2001**, *107*, 48-55.
- 33. Grimme, S.; Antony, J.; Ehrlich, S.; Krieg, H., A consistent and accurate ab initio parametrization of density functional dispersion correction (DFT-D) for the 94 elements H-Pu. *J. Chem. Phys.* **2010**, *132*, 154104.
- 34. Ghosh, A., Substituent Effects on Valence Ionization Potentials of Free Base Porphyrins: A Local Density Functional Study. *J. Am. Chem. Soc.* **1995**, *117*, 4691-4699.
- 35. Ghosh, A., Theoretical Comparative Study of Free Base Porphyrin, Chlorin, Bacteriochlorin, and Isobacteriochlorin: Evaluation of the Potential Roles of ab Initio Hartree–Fock and Density Functional Theories in Hydroporphyrin Chemistry. *J. Phys. Chem. B* **1997**, *101*, 3290-3297.

- 36. Ghosh, A.; Vangberg, T., Valence ionization potentials and cation radicals of prototype porphyrins. The remarkable performance of nonlocal density functional theory. *Theor. Chem. Acc.* **1997**, 97, 143-149.
- 37. Pyykkö, P., Relativistic Effects in Chemistry: More Common Than You Thought. *Ann. Rev. Phys. Chem.* **2012**, 63, 45-64.
- 38. Ghosh, A.; Ruud, K., Relativity and the World of Molecules. Am. Sci. 2023, 111, 160-167.
- 39. Chen, H. L.; Ellis, P. E.; Wijesekera, T.; Hagan, T. E.; Groh, S. E.; Lyons, J. E.; Ridge, D. P., Correlation between gas-phase electron affinities, electrode potentials, and catalytic activities of halogenated metalloporphyrins. *J. Am. Chem. Soc.* **1994**, *116*, 1086-1089.
- 40. Preiß, S.; Förster, C.; Otto, S.; Bauer, M.; Müller, P.; Hinderberger, D.; Hashemi Haeri, H.; Carella, L.; Heinze, K., Structure and reactivity of a mononuclear gold(II) complex. *Nat. Chem.* **2017**, *9*, 1249-1255.
- 41. Ou, Z.; Kadish, K. M.; E, W.; Shao, J.; Sintic, P. J.; Ohkubo, K.; Fukuzumi, S.; Crossley, M. J., Substituent Effects on the Site of Electron Transfer during the First Reduction for Gold(III) Porphyrins. *Inorg. Chem.* **2004**, *43*, 2078-2086.
- 42. Preiß, S.; Melomedov, J.; Wünsche Von Leupoldt, A.; Heinze, K., Gold(III) tetraarylporphyrin amino acid derivatives: ligand or metal centred redox chemistry? *Chem. Sci.* **2016**, *7*, 596-610.
- 43. Kadish, K. M.; E, W.; Ou, Z.; Shao, J.; Sintic, P. J.; Ohkubo, K.; Fukuzumi, S.; Crossley, M. J., Evidence that gold(III) porphyrins are not electrochemically inert: Facile generation of gold(II) 5,10,15,20-tetrakis(3,5-di-tert-butylphenyl)porphyrin. *Chem. Commun.* **2002,** 356-357.
- 44. Ghosh, A.; Conradie, J., Rethinking gold(II) porphyrins: an inherent wave distortion. *Comptes Rendus* **2024**, *Online First*, DOI: 10.5802/crchim.264.
- 45. Ghosh, A., Electronic Structure of Corrole Derivatives: Insights from Molecular Structures, Spectroscopy, Electrochemistry, and Quantum Chemical Calculations. *Chem. Rev.* **2017**, 117, 3798-3881.
- 46. Habenšus, I.; Tomat, E., meso-Aryl substituents modify the electrochemical profile and palladium(II) coordination of redox-active tripyrrin ligands. *Inorg. Chem. Front.* **2024,** *11,* 1789-1798.
- 47. Pérez-Sánchez, J. C.; Herrera, R. P.; Concepción Gimeno, M., Unlocking the catalytic potential of gold(II) complexes: a comprehensive reassessment. *Dalton Trans.* **2024**, *53*, 382-393.
- 48. Witzel, S.; Hashmi, A. S. K.; Xie, J., Light in Gold Catalysis. *Chem. Rev.* **2021**, *121*, 8868-8925.
- 49. Kleinhans, G.; Hansmann, M. M.; Guisado-Barrios, G.; Liles, D. C.; Bertrand, G.; Bezuidenhout, D. I., Nucleophilic T-Shaped (LXL)Au(I)-Pincer Complexes: Protonation and Alkylation. *J. Am. Chem. Soc.* **2016**, *138*, 15873-15876.
- 50. Hicks, J.; Mansikkamäki, A.; Vasko, P.; Goicoechea, J. M.; Aldridge, S., A nucleophilic gold complex. *Nat. Chem.* **2019**, *11*, 237-241.
- 51. Thomas, K. E.; Alemayehu, A. B.; Conradie, J.; Beavers, C.; Ghosh, A., Synthesis and Molecular Structure of Gold Triarylcorroles. *Inorg. Chem.* **2011**, *50*, 12844-12851.
- 52. Thomas, K. E.; Vazquez-Lima, H.; Fang, Y.; Song, Y.; Gagnon, K. J.; Beavers, C. M.; Kadish, K. M.; Ghosh, A., Ligand Noninnocence in Coinage Metal Corroles: A Silver Knife-Edge. *Chem. Eur. J.* **2015**, *21*, 16839-16847.
- 53. Kabsch, W., XDS. Acta Cryst. D 2010, 66, 125-132.
- 54. Sheldrick, G. M., SHELXT Integrated space-group and crystal-structure determination. *Acta Cryst. A* **2015**, *71*, 3-8.
- 55. Bourhis, L. J.; Dolomanov, O. V.; Gildea, R. J.; Howard, J. A. K.; Puschmann, H., The anatomy of a comprehensive constrained, restrained refinement program for the modern computing environment Olex2 dissected. *Acta Cryst. A* **2015**, *71*, 59-75.

- 56. Dolomanov, O. V.; Bourhis, L. J.; Gildea, R. J.; Howard, J. A. K.; Puschmann, H., OLEX2: a complete structure solution, refinement and analysis program. *J. Appl. Cryst.* **2009**, *42*, 339-341.
- 57. Van Lenthe, E.; Baerends, E. J.; Snijders, J. G., Relativistic total energy using regular approximations. *J. Chem. Phys.* **1994**, *101*, 9783-9792.
- 58. Van Lenthe, E.; Ehlers, A.; Baerends, E.-J., Geometry optimizations in the zero order regular approximation for relativistic effects. *J. Chem. Phys.* **1999**, *110*, 8943-8953.
- 59. Becke, A. D., Density-functional thermochemistry. III. The role of exact exchange. *J. Chem. Phys.* **1993**, *98*, 5648-5652.
- 60. Te Velde, G.; Bickelhaupt, F. M.; Baerends, E. J.; Fonseca Guerra, C.; Van Gisbergen, S. J. A.; Snijders, J. G.; Ziegler, T., Chemistry with ADF. *J. Comput. Chem.* **2001**, *22*, 931-967.

For Table of Contents Only



Ligands for Au(III) coordination are enabling new discoveries in homogeneous catalysis, medicinal chemistry, and materials science. Redox-active biopyrrin tripyrrin-1,14-dione stabilizes Au(III) to form square planar complex [Au(TD2)(H_2O)]. Its reversible, one-electron oxidations are ligand-based and access different redox states of the tripyrrindione framework. A primarily metal-based reduction leads to a highly reactive species that utilizes dichloromethane to form a cyclometalated organo-Au(III) complex.